

Journal of Materials Chemistry A

Accepted Manuscript



This is an *Accepted Manuscript*, which has been through the Royal Society of Chemistry peer review process and has been accepted for publication.

Accepted Manuscripts are published online shortly after acceptance, before technical editing, formatting and proof reading. Using this free service, authors can make their results available to the community, in citable form, before we publish the edited article. We will replace this *Accepted Manuscript* with the edited and formatted *Advance Article* as soon as it is available.

You can find more information about *Accepted Manuscripts* in the [Information for Authors](#).

Please note that technical editing may introduce minor changes to the text and/or graphics, which may alter content. The journal's standard [Terms & Conditions](#) and the [Ethical guidelines](#) still apply. In no event shall the Royal Society of Chemistry be held responsible for any errors or omissions in this *Accepted Manuscript* or any consequences arising from the use of any information it contains.



Nanostructured ceramic fuel electrode for efficient CO₂/H₂O electrolysis without safe gas

Yihang Li^a, Pan Li^b, Bobing Hu^a, Changrong Xia^{*a}

Received 00th January 20xx,
Accepted 00th January 20xx

DOI: 10.1039/x0xx00000x

www.rsc.org/

There is increasing interest in converting CO₂/H₂O to syngas via solid oxide electrolysis cells (SOECs) driven by renewable and nuclear energies. The electrolysis reaction is usually conducted through Ni-YSZ (yttria stabilized zirconia) cermets, the state-of-the-art fuel electrodes for SOECs. However, one obvious problem for practical applications is the usage of CO/H₂ safe gas, which must be supplied to maintain the electrode performance. This work reports a safe gas free ceramic electrode for efficient CO₂/H₂O electrolysis. The electrode has a heterogeneously porous structure with Sr₂Fe_{1.5}Mo_{0.5}O_{6-δ} (SFM) electrocatalyst nanoparticles deposited onto the inner surface of YSZ scaffold fabricated by a modified phase-inversion tape-casting method. The nanostructured SFM-YSZ electrodes have demonstrated excellent performance for CO₂-H₂O electrolysis. For example, the electrode polarization resistance is 0.25 Ω cm² under open circuit conditions while the current density is 1.1 A cm⁻² at 1.5 V for the dry CO₂ electrolysis at 800 °C. The performance is comparable with those reported for the Ni-YSZ fuel electrodes, where safe gas must be supplied. In addition, the performance is up to one magnitude better than those reported for other ceramic electrodes such as La_{0.75}Sr_{0.25}Cr_{0.5}Mn_{0.5}O_{3-δ} and La_{0.2}Sr_{0.8}TiO_{3+δ}. Furthermore, the electrode exhibits good stability in the short-term test at 1.3 V for CO₂-20 vol.% H₂O co-electrolysis, which produces a syngas with H₂/CO ratio close to 2. The reduced interfacial polarization resistance, high current density, and good stability show that the nanostructured SFM-YSZ fuel electrode is highly effective for CO₂/H₂O electrolysis without using the safe gas, which is critical for practical applications.

Introduction

The increase of carbon dioxide concentration in the atmosphere has led to many environmental problems, such as global warming, sea level rising, etc.^{1,2} In order to reduce the CO₂ emission into the atmosphere, there has been a worldwide interest in CO₂ capture, storage and utilization in recent years. Consequently, various techniques including multiple chemical and electrochemical methods have been investigated for the conversion and utilization of CO₂. Among these methods, it has been demonstrated that solid oxide electrolysis cell (SOEC) can be a promising candidate to this challenge, combined with electricity energy and heat from nuclear energy or other renewable energy sources such as solar and wind.^{3,4} Driven by the external voltage, SOEC can electrolyze CO₂ and H₂O to produce syngas, a mixture of CO and H₂, which is the precursor of a myriad of high added value industrial products including methane, diesel, methanol etc.^{5,6}

Meanwhile, the released oxygen ions can transport through the ion conducting solid oxide electrolyte and form pure O₂ at the oxygen electrode.^{7,8} Compared to the conventional syngas production method, SOEC does not consume any fossil fuels, showing the maximum efficiency and minimum pollution. Therefore, SOECs may play an important role in stabilizing the carbon cycle and sustainable development.^{4,9,10}

SOEC is usually operated with H₂ and/or CO as the safe gas since the state-of-the-art fuel electrode consists of Ni metal and yttria-stabilized zirconia (YSZ), an oxygen-ion conducting electrolyte.¹¹⁻¹⁴ Without the safe gas, Ni particles undergo the surface oxidation and agglomeration in high CO₂-steam atmosphere, losing its electrical and catalytic activity, leading to poor redox stability, and eventually degrading the cell performance.¹⁵⁻¹⁷ However, using safe gas is not economical and practical in industrial production.¹⁸ Therefore, it is of great interest to develop CO₂ electrolysis and CO₂-H₂O co-electrolysis techniques without the addition of CO/H₂. Theoretically, this could be achieved by using precious metals and redox stable ceramics as the fuel electrodes, which must be chemically stable in the atmospheres from CO₂/H₂O to CO/H₂ at high temperatures up to 900 °C. In such harsh conditions, chemically stable ceramics with mixed oxide-ion electron conductivities are limited to only a few oxides, including La_{0.75}Sr_{0.25}Cr_{0.5}Mn_{0.5}O_{3-δ} (LSCM), La_{0.8}Sr_{0.2}Sc_xMn_{1-x}O_{3-δ}, La_xSr_{1-x}TiO_{3+δ} (LST), Sr₂MgMoO_{6-δ}, La_{0.7}Sr_{0.3}VO_{3-δ} (LSV), and Sr₂Fe_{1.5}Mo_{0.5}O_{6-δ} (SFM).¹⁹⁻²⁵ Among these materials, LSCM, LST have been studied for CO₂ and steam electrolysis without

^a Key Laboratory of Materials for Energy Conversion, Chinese Academy of Sciences, Department of Materials Science and Engineering & Collaborative Innovation Center of Suzhou Nano Science and Technology, University of Science and Technology of China, No. 96 Jinzhai Road, Hefei, Anhui Province, 230026, P. R. China

E-mail: xiacr@ustc.edu.cn

^b Department of Chemistry, University of Science and Technology of China, No. 96 Jinzhai Road, Hefei, Anhui Province, 230026, P. R. China
Electronic Supplementary Information (ESI) available:
See DOI: 10.1039/x0xx00000x

using the safe gas.^{11, 26-29} M.Torrell et al. have prepared a symmetrical cell with LSCM electrodes and 165- μm -thick YSZ electrolyte for CO_2 - H_2O co-electrolysis. At 850 $^\circ\text{C}$, the cell showed a current density of 0.3 A cm^{-2} at 1.5 V when CO_2 -50% H_2O gas mixture was applied to the fuel electrode.³⁰ Xie et al. have fabricated a 700- μm -thick YSZ supported cell with $(\text{La}_{0.2}\text{Sr}_{0.8}\text{TiO}_{3+\delta})$ -GDC ($\text{Gd}_{0.1}\text{Ce}_{0.9}\text{O}_{2-\delta}$) as the fuel electrode and $(\text{La}_{0.8}\text{Sr}_{0.2})_{0.95}\text{MnO}_{3-\delta}$ -GDC as the oxygen electrode. At 700 $^\circ\text{C}$ and 1.5 V, a current density of 0.04 A cm^{-2} was reported for the co-electrolysis of CO_2 -33.3% H_2O .²⁷ It is noted that these cells have shown performance far lower than a typical cell with the Ni-YSZ electrode. For example, at 850 $^\circ\text{C}$ and 1.3 V, a current density as high as 1.0 A cm^{-2} is achieved for the co-electrolysis of a gas mixture of 25% CO_2 -25% H_2O -25% CO -25% Ar .¹²

In this study, a heterogeneously porous SFM-YSZ fuel electrode is developed for CO_2 and steam electrolysis without using the safe gas. The simplified microstructure is schematically shown in Fig.1, where CO_2 and H_2O are expected to be converted to CO and H_2 . The electrolyte is YSZ while the electrocatalyst is double perovskite SFM, which has been studied as the symmetrical electrode materials for solid oxide electrolysis cells due to its excellent catalytic activity in temperature range of 750-850 $^\circ\text{C}$.²⁹ The YSZ scaffold is formed using a modified phase-inversion tap-casting method while the SFM electrocatalyst by the infiltration technique to avoid the possible solid state reactions between SFM and YSZ since SFM is proven to be chemical compatible with YSZ only below 1000 $^\circ\text{C}$.³¹ The infiltration derived SFM nanoparticles are uniformly deposited on the internal surfaces of the YSZ scaffold consisting of a gas delivery layer with unique finger-like large pores and electrochemical reaction layer with small pores and high surface area. The novel nanostructured electrode demonstrates a remarkable performance without the safe gas, comparable to the state-of-the-art Ni-YSZ electrode, which must be operated with the safe gas.

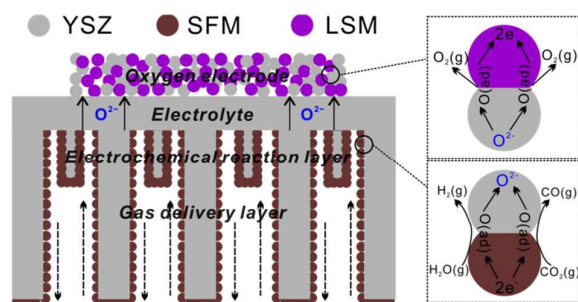


Fig.1 A schematic diagram for $\text{CO}_2/\text{H}_2\text{O}$ electrolysis without using the safe gas.

Experimental

YSZ (8% mol yttria-stabilized zirconia, TZ-8Y, Tosoh Corporation) porous substrate was fabricated by the phase-inversion tape-casting method, which was modified with a graphite layer to remove the sponge layer,^{32,33} as described in

Fig.S1 and Table S1 of the Supplementary Information. The white tape was cut into disc samples of diameter 13 mm and dried in an oven for 30 min, following by heating 1200 $^\circ\text{C}$ for 2 h with the heating rate of 3 $^\circ\text{C}\cdot\text{min}^{-1}$ for form porous YSZ substrates. Typically, the 7 wt. % YSZ (TZ-8Y, Tosoh co., Japan) with the mean particle size of 0.1 μm was dispersed in ethanol and ball-milled for 24 h. The YSZ suspension was dripped on the center of the YSZ substrate, which was immediately spun at 2000 rpm for 30 s to form a thin, uniform YSZ layer. After drying at room temperature, another dripping-cycle was done. The thickness of 10 μm was achieved by 5 cycles. Then it was sintered at 1400 $^\circ\text{C}$ for 5 h with the heating rate of 3 $^\circ\text{C}\cdot\text{min}^{-1}$, resulting in a bi-layer structure consisting of a porous YSZ substrate layer and a dense YSZ film layer. LSM ($(\text{La}_{0.85}\text{Sr}_{0.15})_{0.9}\text{Mn}_{3-\delta}$) powder was prepared by a glycine-nitrate combustion method with the glycine/metal ratio of 1.15.³⁴ The precursor solution was heated until self-combustion occurred. The as-prepared powder was collected and calcined at 1100 $^\circ\text{C}$ for 2 h in air with the heating rate of 3 $^\circ\text{C}\cdot\text{min}^{-1}$. LSM-YSZ (weight ratio of 6:4) powders were mixed with 50 wt% binders and solvent and grinded in an agate mortar for 1 h. The paste was printed on the surface of the electrolyte by screen printing method, followed by heating at 1200 $^\circ\text{C}$ for 2 h with the heating rate of 3 $^\circ\text{C}\cdot\text{min}^{-1}$ to form a tri-layer structure with a porous YSZ substrate, a dense YSZ film, and a porous LSM-YSZ. An aqueous solution containing Sr^{2+} , Fe^{3+} , and Mo^{6+} ions was prepared by dissolving their soluble salts ($\text{Sr}(\text{NO}_3)_2$, $\text{Fe}(\text{NO}_3)_3\cdot 9\text{H}_2\text{O}$, and $(\text{NH}_4)_6\text{Mo}_7\text{O}_{24}\cdot 4\text{H}_2\text{O}$) (99.9%, Sinopharm Chemical Reagent Co., Ltd) in deionized water with a molar ratio of $\text{Sr}^{2+}:\text{Fe}^{3+}:\text{Mo}^{6+} = 2:1.5:0.5$. The total metal ion concentration was 1.2 M in the $\text{Sr}_2\text{Fe}_{1.5}\text{Mo}_{0.5}\text{O}_{6-\delta}$ precursor solution. Citric acid and glycine were added into the SFM solution as the complexing reagents and combustion agents with a molar ratio of citric acid: glycine: metal cations = 1.5: 2: 1. The SFM deposition was conducted by infiltrating the precursor solution into the porous YSZ substrate under vacuum circumstance, followed by heating at 600 $^\circ\text{C}$ for 1 h with the heating rate of 3 $^\circ\text{C}\cdot\text{min}^{-1}$. The process was repeated to increase the SFM loadings to 20 wt.% (relative to the quality of the YSZ scaffold). Finally, the cell was heated at 850 $^\circ\text{C}$ for 5 h with the heating rate of 3 $^\circ\text{C}\cdot\text{min}^{-1}$ to obtain crystallized $\text{Sr}_2\text{Fe}_{1.5}\text{Mo}_{0.5}\text{O}_{3-6}$, resulting in a single cell consisting of a SFM-YSZ fuel electrode, a YSZ electrolyte, and a LSM-YSZ oxygen electrode, Fig.1.

The single cell was sealed on the end of an alumina ceramic tube with conductive resins (Shanghai Institute of synthetic resin, DAD87) in a verticle furnace (Fig.S2). Ag wires and Ag pastes were used as the current and voltage probes. The electrochemical performance was tested in both fuel cell and electrolysis modes using humidified hydrogen and carbon dioxide (99.8%, Nanjing special gas Factory Co., Ltd.), respectively. Steam was supplied via bubbling through water at controlled temperature. The gas flow rate was kept at 20 ml min^{-1} using a mass flow controller (D08-2F, Qixing Huachuang Co., Ltd.). The current-voltage characteristics were measured from open circuit voltage to 1.5 V with a scanning rate of 20 mV s^{-1} . The AC impedance measurements were carried out

with an electrochemical interface (Solartron 1287) combined with a frequency response analyzer (Solartron 1260). The frequency ranged typically from 10^6 Hz to 10^{-2} Hz with amplitude of 10 mV. The microstructures were examined using a field emission scanning electron microscopy, equipped with EDX (SEM, JEOL JSM-6700 F), and transition electron microscope (TEM, JEOL JSM-2010). The mercury injection apparatus (Quantachrome PM60GT-17) was employed to measure the pore size distributions. The durability was evaluated by monitoring the current density under constant output voltage or the cell voltage under constant current density. The flow rate of outlet gas was measured with a self-made soap film flow meter. The contents of CO_2 , CO , H_2 were determined by online gas chromatography (FULI, GC9790 II). SFM-YSZ electrode after CO_2 electrolysis was analyzed using Raman spectroscopy (Raman, Lab RAM HR800, $1000\text{--}2000\text{ cm}^{-1}$). Although it was not sure whether CO was generated by the electrolysis reaction or reversible water-gas shift reaction, the total generated gas (CO and H_2) should accomplish the theoretical values. That is to say, we can introduce an important performance parameter, electricity to syngas efficiency (assuming 100% current efficiency).

Results and discussion

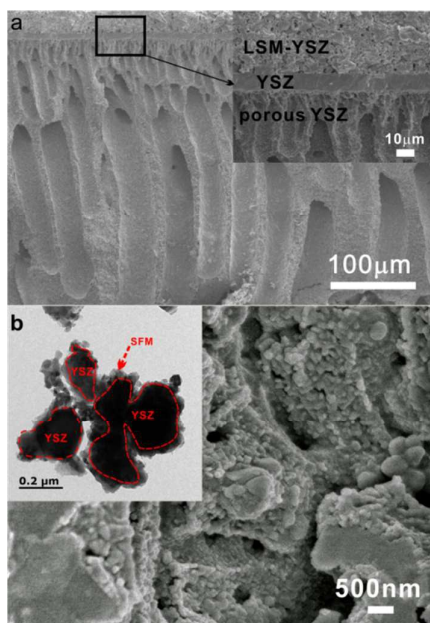


Fig.2 The cell microstructures (a) cross-sectional SEM image of a porous YSZ scaffold and a tri-layer structure consisting of a porous YSZ, a dense YSZ and a porous LSM-YSZ layer, the up-right inset and (b) SEM image for the SFM-YSZ electrode and TEM picture showing the fine structure, the up-left inset.

Fig. 2 presents the microstructures of a single cell with a SFM-YSZ fuel electrode, a 10- μm -thick YSZ electrolyte and a LSM-YSZ oxygen electrode. Fig. 2a shows that the YSZ substrate has a graded open

pore structure along the thickness direction, where large finger-like pores far from the electrolyte facilitate gas delivery, while small finger-like pores, adjacent to the electrolyte, serve as the functional layer for electrochemical reactions, see also Fig.1 and Fig.S3. The graded structure has a tri-polar pore size distribution, 10-100 μm large pores, 0.2-1 μm small pores, and 15-30 nm fine pores, Fig.3. The up-right inset of Fig. 2a exhibits very good bonding between the dense YSZ and porous layers. Fig. 2b shows that the YSZ scaffold is covered with SFM particles, which forms a highly continuous network for electronic conduction. The particle size is 30-50 nm, as confirmed by the bright field TEM image in the up-left inset of Fig. 2b. The nanoparticles have a good contact with the YSZ scaffold, forming some bigger aggregates. In addition to Zr and Y, Sr, Fe and Mo elements present in the infiltrated electrode as revealed with the energy dispersive X-ray mapping, Fig.S4. Sr, Fe and Mo elements are found at the electrode-electrolyte interface, demonstrating that the vacuum-assistant infiltration is effective to introduce SFM particles to the interface between the porous and dense YSZ layers throughout the 700 μm thick scaffold. Furthermore, the nanoparticles do not have obvious effect on the pore size distribution, while slightly reduces the size of the large, small, and fine pores, Fig. 3, suggesting that SFM could be deposited to every available inner surface of the YSZ scaffold. The shrinkage in pore size is accompanied with pore volume reduction, which is also shown with porosity reduction from 57% to 50% by the Archimedes drainage method. The tortuosity factor of SFM-YSZ fuel electrode is determined to be 2.03 by the mercury intrusion method, much lower than the values of 6-10 for the traditional fuel electrodes.^{35, 36} The nanoparticles are double perovskite structured SFM when the infiltrates are heated at 850 $^{\circ}\text{C}$, Fig.S5. The XRD analysis also suggests that SFM is chemically compatible with YSZ below 850 $^{\circ}\text{C}$. Excellent electrochemical performance is expected for this unique structure where straight open pores facilitate gas delivery and SFM nanoparticles promote the electrode reaction.

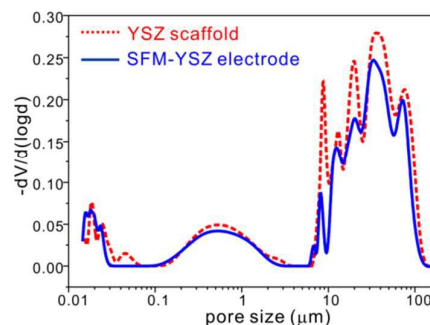


Fig.3 The pore size distribution of a YSZ scaffold and a SFM-YSZ electrode.

The electrochemical performance of the nanostructured SFM-YSZ electrode is investigated in both fuel cell and electrolysis modes. The fuel cell mode is conducted with humidified hydrogen (~ 3 vol.% H_2O) as the fuel and ambient air as the oxidant, Fig. 4. The open circuit voltage (V_{oc}) is 1.04 V at 800 $^{\circ}\text{C}$, indicating that the YSZ electrolyte is dense enough. The peak power density is 1.03 W cm^{-2} while the total interfacial polarization resistance is only $0.18\ \Omega\text{ cm}^2$

under open circuit conditions. The SFM-YSZ electrode polarization resistance is about $0.02 \Omega \text{ cm}^2$ considering that the LSM-YSZ electrode resistance is $0.16 \Omega \text{ cm}^2$ as determined with a LSM-YSZ | YSZ | LSM-YSZ symmetrical cell measured in air, Fig.S7. The electrochemical performance is much higher than those reported for SFM based fuel electrodes. For example, the polarization resistance of a SFM fuel electrode supported on a LSGM electrolyte is $0.27 \Omega \text{ cm}^2$.²³ Considering that LSGM has relatively higher ionic conductivity than YSZ, the polarization resistance of the nanostructured SFM should be even lower when it is applied on the LSGM electrolyte. The performance is even comparable with that obtained using the Ni-YSZ electrode, which is also prepared with the phase-inversion tape-casting method. The peak power density is 0.80 W cm^{-2} at 800°C for a single cell consisting of a Ni-YSZ fuel electrode, a $10\text{-}\mu\text{m}$ thick YSZ electrolyte and a LSM-YSZ oxygen electrode.³² Such excellent performance should be attributed to the novel structure where graded YSZ scaffold is infiltrated with SFM nanoparticles. Furthermore, the single cell is very stable in 60-hour testing at 800°C with only 3.7% degradation in the current, Fig.4c.

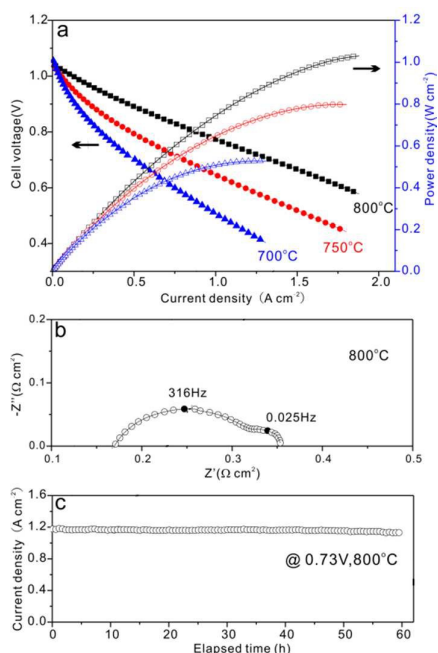


Fig.4 The electrochemical performance of a single cell with the SFM-YSZ fuel electrode tested in fuel cell mode with humidified H_2 as the fuel and ambient air as the oxidant. (a) Cell voltage and power density as a function of current density; (b) Electrochemical impedance spectra measured under open circuit conditions; (c) Durability test at the constant cell voltage of 0.73V

The electrochemical performance is further investigated in electrolysis mode by electrolyzing H_2O and using H_2 as the safe gas, Fig.5. In the electrolysis mode, negative current density indicates that steam is split into hydrogen and oxygen. The V_{oc} increases with the increase of H_2 concentration, i.e., the decrease in H_2O concentration, which can be described by the Nernst Equation.¹⁶ At V_{oc} , the total interfacial resistance is $0.230 \Omega \text{ cm}^2$, $0.245 \Omega \text{ cm}^2$ and $0.263 \Omega \text{ cm}^2$ while the SFM-YSZ electrode resistance is $0.07 \Omega \text{ cm}^2$, $0.085 \Omega \text{ cm}^2$ and $0.103 \Omega \text{ cm}^2$ obtained respectively with 10vol.

H_2O , 20vol. H_2O and 30vol. H_2O . The applied voltage increases almost linearly with the increasing current density up to 1.5 A cm^{-2} , showing no concentration polarization, which could be ascribed to the unique microstructure of the SFM-YSZ electrode. At the applied voltage of 1.3 V, a current density of 1.12 A cm^{-2} is observed for 10vol.% H_2O , while it increases to 1.27 A cm^{-2} for 20vol.% H_2O and 1.35 A cm^{-2} for 30vol.% H_2O . In general, the steam electrolysis performance is improved significantly compared with previous reports which are tested under the similar conditions. For example, the total interfacial polarization resistance based on the YSZ electrolyte is $0.245 \Omega \text{ cm}^2$, comparing to $0.65 \Omega \text{ cm}^2$ for a SFM electrode on LSGM electrolyte tested at 800°C for steam electrolysis of H_2 -20vol.% H_2O .³⁷ In addition, the performance is comparable to those of the Ni-YSZ supported cells, e.g., $0.22 \Omega \text{ cm}^2$ at V_{oc} and 1.7 A cm^{-2} at 1.3 V for 50 vol.% H_2O for a Ni-YSZ/YSZ/LSM-YSZ cell.^{38, 39} Furthermore, the electrolysis cell is stable during the short-term durability testing for steam electrolysis at constant current density of 1.0 A cm^{-2} and 1.5 A cm^{-2} , Fig.5c. As discussed above, the SFM infiltrated YSZ composite electrode can effectively improve the catalytic activity for steam electrolysis.

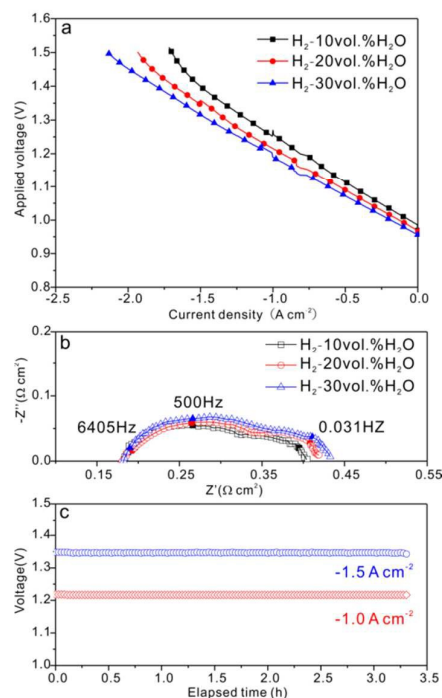


Fig.5 The electrochemical performance at 800°C for a single cell with the SFM-YSZ fuel electrode tested by electrolyzing steam and with humidified H_2 as the safe gas. (a) Applied voltage as a function of current density; (b) Electrochemical impedance spectra under open circuit conditions; (c) The variation of cell voltage versus time in the galvanostatic mode using H_2 -20vol.% H_2O

Subsequently, the SFM-YSZ electrode is applied for dry CO_2 electrolysis and CO_2 - H_2O co-electrolysis without using the safe gas, either H_2 or CO , Fig.6. When no H_2/CO is used, the V_{oc} becomes much lower, consistent with previous reports.^{40, 41} As the applied voltage reaches theoretical V_{oc} , the electrolysis reaction can proceed. Then, the applied voltage increases sharply with the

current density, having an obvious turning point for each curve. The high turning point is a reflection of the catalytic activity of SFM for CO₂ and water splitting. Below the turning point, the applied voltage increases sharply with the current density, which is possibly associated with the electrochemical reduction of SFM, i.e., the activation process of SFM electrocatalyst.^{28, 42} When the applied voltage exceeds the turn point, the electrochemical reduction of CO₂ and H₂O starts to accelerate at an exponential rate in the current density, indicating that the increased voltage promotes the reaction kinetics significantly.

When dry CO₂ is electrolyzed, the SFM-YSZ electrode demonstrates excellent performance comparing to those reported for single cells based on YSZ electrolytes and safe-gas free electrodes, Table 1. At 1.5 V, the current density is 1.10 A cm⁻², which is 57% higher than 0.7 A cm⁻², the highest current density

that has been reported for CO₂ electrolysis without using the safe gas. Comparing with the cells using the LST-SDC and LSCM-SDC composites, typical safe-gas free fuel electrodes, the current density is increased by a factor up to 20. The total interfacial polarization resistance at Voc is 0.41 Ω cm², much smaller than 3.2 Ω cm² and 12 Ω cm² for the LSCM-SDC and LST-SDC based single cells, respectively. The SFM-YSZ electrode resistance is only 0.25 Ω cm², one order of magnitude lower than the LSCM-SDC and LST-SDC electrodes when the same oxygen electrode resistance is assumed. Also, the performance is comparable to those reported for the Ni-YSZ based cells, which must be operated with the safe gas. For example, when 10% CO is used as the safe gas, the interfacial polarization resistance is 0.32 Ω cm² at Voc and the current density is 0.45 A cm⁻² at 1.5V for a Ni-YSZ based cell that is operated at 900 °C.⁷ Therefore, SFM-YSZ has demonstrated the highest performance as fuel electrode for dry CO₂ electrolysis.

Table 1 Current density at 1.5V and total interfacial polarization resistance for pure CO₂ electrolysis using different fuel electrodes that are operated at 800 °C.

Fuel electrode	YSZ Electrolyte thickness	Oxygen electrode	Polarization resistance (Ω cm ²)	Current density (A cm ⁻²)
Pt/YSZ	325 μm	Pt/YSZ	-	0.08 ⁴³
LSCM-SDC	2 mm	LSCM-SDC	3.2 at Voc	0.09 ⁴⁴
Cu-LSCM-SDC	2 mm	LSCM-SDC	0.9 at 1.2 V	0.5 ⁴⁵
Ni-LSCM-SDC	1 mm	LSM-SDC	1.45 at 1.2 V	0.2 ⁴¹
LST-SDC	2 mm	LSM-SDC	12 at Voc	0.05 ⁴⁶
LSTM ^a -SDC	2 mm	LSM-SDC	1.52 at 1.2 V	0.15 ⁴⁰
Ag-SDC	0.13 mm	LSM-YSZ	1.25 at Voc	0.7 ⁴²
SFM-YSZ	10 μm	LSM-YSZ	0.41 at Voc	1.1 (Present)

Note: LSTM^a = La_{0.2}Sr_{0.8}Ti_{0.9}Mn_{0.1}O_{3-δ}

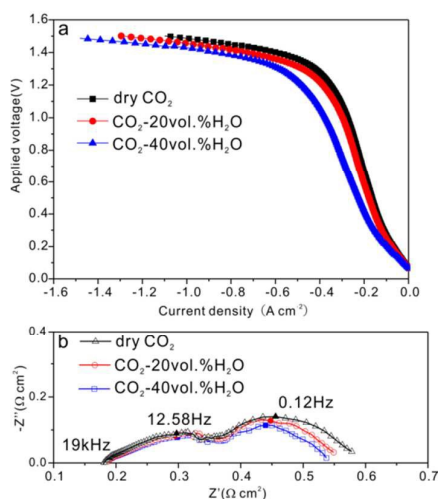
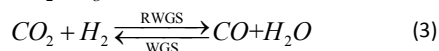
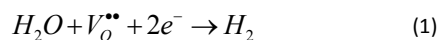


Fig.6 The performance for CO₂ electrolysis and CO₂-H₂O co-electrolysis at 800 °C without the safe gas. (a) Applied voltage as a function of current density; (b) Electrochemical impedance spectra under open circuit conditions.

When steam is added, the cell exhibits better performance, Fig. 6a. The turn point is observed at slightly lower applied voltage, which can be attributed to the relatively lower decomposition potential of steam than that of CO₂.⁴ The current density is increased with the increasing steam concentration. For example, when the applied voltage is 1.5 V, the current density is increased from 1.10 A cm⁻² for dry CO₂, to 1.27 A cm⁻² for CO₂-20vol.% H₂O, and further to 1.46 A cm⁻² for CO₂-40vol.% H₂O. Meanwhile, the total polarization resistance under open circuit conditions is reduced from 0.41 Ω cm² to 0.39 Ω cm² and 0.36 Ω cm², respectively. It is reported that steam electrolysis performs easier than CO₂ electrolysis due to less activation energy for adsorption and dissociation as well as the larger diffusion coefficient,³⁹ so the corresponding polarization resistance is reduced, revealing the CO₂ reduction should be probably the limiting step in the CO₂-H₂O co-electrolysis process. The reaction steps of the coelectrolysis reaction in the fuel electrode are very complicated and can be briefly shown as followings:⁴⁷



Apparently, the chemistry involved in the co-electrolysis of steam and CO₂ is significantly more complicated than that involving the steam or CO₂ electrolysis alone. It's beyond the scope of this work, but will be addressed in future work.

The CO₂-H₂O co-electrolysis performance derived from the SFM-YSZ electrode is also compared with that reported in the literatures under similar operating conditions, Table 2. The current density and total interfacial polarization resistance is comparable with those obtained using the Ni-YSZ electrodes, the state-of-the-art fuel electrodes, where H₂ and/or CO must be supplied as the safe gas to maintain the electrochemical performance. The

Table 2 Cell performance for CO₂-steam co-electrolysis using different fuel electrodes

Fuel electrode	Inlet gas CO ₂ /H ₂ O ratio	YSZ electrolyte thickness	Oxygen electrode	Total polarization resistance at Voc (Ω cm ²)	Current density (A cm ⁻²)
Ni-YSZ	1:1 with 25%H ₂	130 μm	LSM-YSZ	0.27	-1.3 at 1.5 V, 800 °C ¹³
Ni-YSZ	1:1 with 10%H ₂	10 μm	LSC ^a -GDC	0.2	-1.5 at 1.2 V, 800 °C ⁴⁸
Pd-oxide ^b	5:3 with 20%CO	80 μm	LSF ^c -YSZ	0.5	-1.5 at 1.5 V, 800 °C ²⁴
LSCM	1:1 without safe gas	165 μm	LSCM	1.5	-0.3 at 1.5 V, 850 °C ⁴⁹
LST-GDC	2:1 without safe gas	700 μm	LSM-GDC	8.5	-0.04 at 1.5 V, 700 °C ²⁷
SFM-YSZ	3:2 without safe gas	10 μm	LSM-YSZ	0.36	-1.46 at 1.5V, 800 °C (Present)

Note: LSC = La_{0.7}Sr_{0.3}CoO_{3-δ}; oxide = CeO₂-LSV-YSZ; LSF = (La_{0.6}Sr_{0.4})_{0.99}FeO_{3-δ}

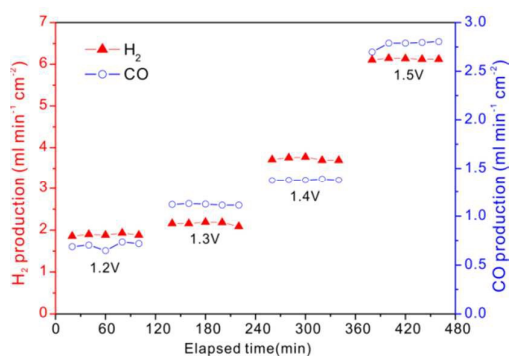


Fig.7 CO and H₂ production from the co-electrolysis of CO₂-20vol.% H₂O at 800 °C under different applied voltages.

Fig.7 shows the production rate derived from CO₂-20vol.% H₂O co-electrolysis at various applied voltages. The rate increases with the applied voltage, consistent with the results show in Fig. 6a. The H₂ production rate is 1.89 ml min⁻¹ cm⁻² at 1.2 V, increasing to 6.12 ml min⁻¹ cm⁻² at 1.5 V. The production rate increases by a factor more than 3 when the voltage is increased from 1.2 V to 1.5 V, suggesting high voltage operation benefits the co-electrolysis process. The CO production rate is 0.72 and 2.80 ml min⁻¹ cm⁻² at 1.2 and 1.5 V, respectively. The CO/H₂ ratio in the product is much lower than the CO₂/H₂O ratio of the feeding gas, suggesting that co-electrolysis process is predominated by steam reduction. The CO/H₂ ratio is also affected by the applied voltage, inferring that the kinetics dependence on the voltage is different for CO₂ and steam. It's thus possible to control the CO/H₂ ratio through the voltage, which is very feasible to realize. At 1.3 V, the CO/H₂ ratio

performance is also comparable with LSV (La_{0.7}Sr_{0.3}VO_{3-δ}) based oxide electrode enhanced with Pd and CeO₂ catalysts and operated using the safe gas. In addition, the performance is much higher than the available reported data on co-electrolysis without using the safe gas. The interfacial polarization resistance at Voc for the SFM-YSZ fuel electrode is 0.20 Ω cm² for CO₂-40vol.% H₂O. It is even 5 times lower than that reported for the LSCM based electrode for CO₂-50vol.% H₂O at 850 °C when the same resistance is assumed for the fuel electrode (0.16 Ω cm²). The current density, 1.46 A cm⁻² at 800 °C for present work, is about 5 times as that of 0.3 A cm⁻² at 850 °C as reported by M. Torrell *et al.*

is closed to 0.5, which is a highly value-added production that is quite desired for the synthetic fuels in the industrial practices of Fischer-Tropsch synthesis.⁵⁰

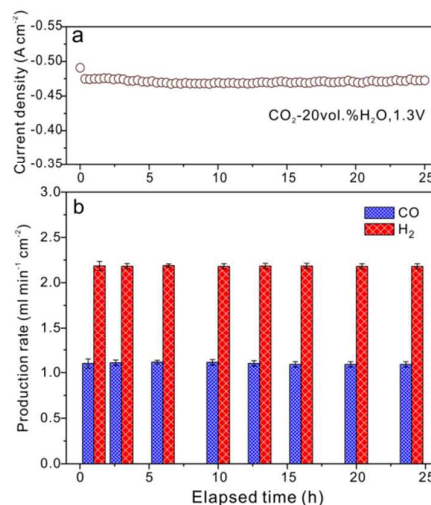


Fig.8 Short-term performance test for CO₂-20vol.% H₂O co-electrolysis under applied potential of 1.3V. (a) Current density versus elapsed time; (b) Production rates of CO and H₂ (The error bars represent the standard deviations of three independent measurements)

The variation of current density via elapsed time is recorded for CO₂-20 vol.% H₂O co-electrolysis at 800 °C under a constant

applied voltage of 1.3 V, Fig.8a. The initial current density is in good agreement with the value observed in Fig.6a. In the initial stage of 5 h, there is a slight decline in the current density, about 0.0016 A cm⁻² per hour. Subsequently, there is no observable degradation in the current density, indicating a steady state operation has been achieved after 5 h operation.⁵¹ The production rate is also measured with the interval of 2-5 h, Fig. 8b. The total amount of generated CO/H₂ gas in Fig.8b, which is determined with the gas chromatography from the outlet stream, is about 96.5% of the predicted value from the current density shown in Fig.8a. The inconsistency phenomenon should be related to O₂ impurities at the fuel electrode side as well as the gas leakage.⁵² It is worth noting that the H₂/CO ratio is kept at about 2:1, which could readily serve as the feedstock for the synthesis of alcohols, and other liquid fuels.

Conclusions

In this work, the SFM-YSZ electrode has demonstrated excellent electrochemical performance. In the fuel cell mode, a electrode interfacial polarization resistance of 0.02 Ω cm⁻² and a peak power density of 1.03 W cm⁻² are achieved at 800 °C when humidified H₂ is used as the fuels. In the electrolysis mode, the interfacial polarization resistances of the fuel electrode are 0.25 Ω cm² and 0.20 Ω cm² under open circuit conditions while the current densities are 1.10 A cm⁻² and 1.46 A cm⁻² for the electrolysis of dry CO₂ and the co-electrolysis of CO₂-40vol.% H₂O, respectively, when the cell is operated at 800 °C under the applied voltage of 1.5 V. The performance is comparable with Ni-YSZ cermet, the state-of-the-art fuel electrode, which must be operated with safe gas of CO/H₂. In addition, the electrolysis performance is much higher than that reported for other ceramic electrodes operated without the safe gas. For example, when dry CO₂ is electrolyzed at 800 °C, the current is enlarged by a factor up to 20 while the interfacial polarization resistance is reduced to one magnitude lower. During 25 h stability test for CO₂-20vol.% H₂O co-electrolysis at 1.3 V, the cell has achieved a stable production rate and H₂/CO ratio of approximate 2, which is suitable for synthesizing hydrocarbon fuels. The excellent electrochemical performance should be resulted from the unique electrode structure where the large finger-like channel benefits the fuel delivery efficiency while the small finger-like layer adjacent to electrolyte benefits the electrochemical reactions, which is further enhanced with SFM nanoparticles that are capable of catalyzing CO₂-H₂O electrolysis without addition of any safe gases. Further, the SFM-YSZ electrode does not show any reactant starvation phenomena that could be observed for the conventional composite fuel electrodes. In short, this study reveals that the nanostructured ceramic fuel electrode is a promising strategy for CO₂/H₂O electrolysis without the safe gas.

Acknowledgements

This work has been financially supported by the Ministry of Science and Technology of China (2012CB215403) and the National Natural Science Foundation of China (51372239).

Notes and references

- J. M. Valverde, *J Mater Chem A*, 2013, **1**, 447-468.
- S. J. Davis, K. Caldeira and H. D. Matthews, *Science*, 2010, **329**, 1330-1333.
- L. Bi, S. Boulfrad and E. Traversa, *Chemical Society Reviews*, 2014, **43**, 8255-8270.
- S. D. Ebbesen, S. H. Jensen, A. Hauch and M. B. Mogensen, *Chem Rev*, 2014, **114**, 10697-10734.
- L. Chen, F. L. Chen and C. R. Xia, *Energ Environ Sci*, 2014, **7**, 4018-4022.
- Z. Jiang, T. Xiao, V. L. Kuznetsov and P. P. Edwards, *Philos T R Soc A*, 2010, **368**, 3343-3364.
- X. L. Yue and J. T. S. Irvine, *J Electrochem Soc*, 2012, **159**, F442-F448.
- Y.-Q. Zhang, J.-H. Li, Y.-F. Sun, B. Hua and J.-L. Luo, *ACS Appl Mater Inter*, 2016, **8**, 6457-6463.
- A. Midilli and I. Dincer, *Int J Hydrogen Energy*, 2007, **32**, 511-524.
- C. Graves, S. D. Ebbesen, M. Mogensen and K. S. Lackner, *Renewable and Sustainable Energy Reviews*, 2011, **15**, 1-23.
- R. M. Xing, Y. R. Wang, Y. Q. Zhu, S. H. Liu and C. Jin, *J Power Sources*, 2015, **274**, 260-264.
- S. D. Ebbesen, R. Knibbe and M. Mogensen, *J Electrochem Soc*, 2012, **159**, F482-F489.
- C. H. Yang, J. Li, J. Newkirk, V. Baish, R. Z. Hu, Y. Chen and F. L. Chen, *J Mater Chem A*, 2015, **3**, 15913-15919.
- Y. Li, L. Chen, L. Zhang and C. Xia, *Int J Hydrogen Energy*, 2016, **41**, 5209-5214.
- S. D. Kim, D. W. Seo, A. K. Dorai and S. K. Woo, *Int J Hydrogen Energy*, 2013, **38**, 6569-6576.
- C. Jin, C. H. Yang and F. L. Chen, *J Electrochem Soc*, 2011, **158**, B1217-B1223.
- S. D. Ebbesen and M. Mogensen, *J Power Sources*, 2009, **193**, 349-358.
- Q. X. Fu, C. Mabilat, M. Zahid, A. Brisse and L. Gautier, *Energ Environ Sci*, 2010, **3**, 1382-1397.
- S. Sengodan, H. J. Yeo, J. Y. Shin and G. Kim, *J Power Sources*, 2011, **196**, 3083-3088.
- D. Neagu and J. T. S. Irvine, *Chem Mater*, 2010, **22**, 5042-5053.
- J. C. Ruiz-Morales, J. Canales-Vazquez, C. Savaniu, D. Marrero-Lopez, W. Z. Zhou and J. T. S. Irvine, *Nature*, 2006, **439**, 568-571.
- Y. H. Huang, R. I. Dass, Z. L. Xing and J. B. Goodenough, *Science*, 2006, **312**, 254-257.
- Q. A. Liu, X. H. Dong, G. L. Xiao, F. Zhao and F. L. Chen, *Advanced Materials*, 2010, **22**, 5478-5482.
- S. E. Yoon, S. H. Song, J. Choi, J. Y. Ahn, B. K. Kim and J. S. Park, *Int J Hydrogen Energy*, 2014, **39**, 5497-5504.
- S. W. Tao and J. T. S. Irvine, *Nat Mater*, 2003, **2**, 320-323.
- X. L. Yue and J. T. S. Irvine, *Solid State Ionics*, 2012, **225**, 131-135.
- K. Xie, Y. Q. Zhang, G. Y. Meng and J. T. S. Irvine, *Energ Environ Sci*, 2011, **4**, 2218-2222.
- S. S. Li, Y. X. Li, Y. Gan, K. Xie and G. Y. Meng, *J Power Sources*, 2012, **218**, 244-249.
- Y. Wang, T. Liu, S. Fang and F. Chen, *J Power Sources*, 2016, **305**, 240-248.
- M. Torrell, S. García-Rodríguez, A. Morata, G. Penelas and A. Tarancón, *Faraday discussions*, 2015, **182**, 241-255.
- L. dos Santos-Gómez, L. Leon-Reina, J. Porras-Vazquez, E. Losilla and D. Marrero-López, *Solid State Ionics*, 2013, **239**, 1-7.

ARTICLE

Journal Name

- 32 H. Huang, J. Lin, Y. L. Wang, S. R. Wang, C. R. Xia and C. S. Chen, *J Power Sources*, 2015, **274**, 1114-1117.
- 33 L. Chen, M. T. Yao and C. R. Xia, *Electrochem Commun*, 2014, **38**, 114-116.
- 34 R. Peng, X. Fan, Z. Jiang and C. Xia, *Fuel Cells*, 2006, **6**, 455-459.
- 35 E. L. Cussler, *Diffusion: mass transfer in fluid systems*, Cambridge university press, 2009.
- 36 Y. Chen, Y. X. Zhang, J. Baker, P. Majumdar, Z. B. Yang, M. F. Han and F. L. Chen, *Acs Appl Mater Inter*, 2014, **6**, 5130-5136.
- 37 Q. A. Liu, C. H. Yang, X. H. Dong and F. L. Chen, *Int J Hydrogen Energ*, 2010, **35**, 10039-10044.
- 38 C. H. Yang, C. Jin and F. L. Chen, *Electrochim Acta*, 2010, **56**, 80-84.
- 39 Z. Zhan, W. Kobsiriphat, J. R. Wilson, M. Pillai, I. Kim and S. A. Barnett, *Energ Fuel*, 2009, **23**, 3089-3096.
- 40 W. T. Qi, Y. Gan, D. Yin, Z. Y. Li, G. J. Wu, K. Xie and Y. C. Wu, *J Mater Chem A*, 2014, **2**, 6904-6915.
- 41 C. Ruan and K. Xie, *Catal Sci Technol*, 2015, **5**, 1929-1940.
- 42 Y. M. Xie, J. Xiao, D. D. Liu, J. Liu and C. H. Yang, *J Electrochem Soc*, 2015, **162**, F397-F402.
- 43 G. Tao, K. R. Sridhar and C. L. Chan, *Solid State Ionics*, 2004, **175**, 621-624.
- 44 S. S. Xu, S. S. Li, W. T. Yao, D. H. Dong and K. Xie, *J Power Sources*, 2013, **230**, 115-121.
- 45 H. X. Li, G. H. Sun, K. Xie, W. T. Qi, Q. Q. Qin, H. S. Wei, S. G. Chen, Y. Wang, Y. Zhang and Y. C. Wu, *Int J Hydrogen Energ*, 2014, **39**, 20888-20897.
- 46 Y. X. Li, J. E. Zhou, D. H. Dong, Y. Wang, J. Z. Jiang, H. F. Xiang and K. Xie, *Phys Chem Chem Phys*, 2012, **14**, 15547-15553.
- 47 H. N. Im, S. Y. Jeon, D. K. Lim, B. Singh, M. Choi, Y. S. Yoo and S. J. Song, *J Electrochem Soc*, 2015, **162**, F54-F59.
- 48 P. Hjalmarsen, X. F. Sun, Y. L. Liu and M. Chen, *J Power Sources*, 2014, **262**, 316-322.
- 49 M. Torrell, S. García-Rodríguez, A. Morata, G. Penelas and A. Tarancon, *Faraday Discussions*, 2015.
- 50 Q. H. Zhang, J. C. Kang and Y. Wang, *Chemcatchem*, 2010, **2**, 1030-1058.
- 51 C. H. Yang, Z. B. Yang, C. Jin, M. L. Liu and F. L. Chen, *Int J Hydrogen Energ*, 2013, **38**, 11202-11208.
- 52 G. Tao, K. R. Sridhar and C. L. Chan, *Solid State Ionics*, 2004, **175**, 615-619.